Microscopic Interpretation of the Payne Effect in Model Fractal-Aggregate Polymer Nanocomposite

Yang Wang, Gaëtan Maurel, Marc Couty, François Detcheverry, Samy Merabia

Microscopic Interpretation of the Payne Effect in Model Fractal-Aggregate Polymer Nanocomposite

Yang Wang[1,2], Gaëtan Maurel[2], Marc Couty[2], François Detcheverry[1,*] and Samy Merabia[1,*]
[1] *University of Lyon, Université Claude Bernard Lyon 1, CNRS, Institut Lumière Matière, F-69622 Villeurbanne, France and*
[2] *MFP MICHELIN 23, Place des Carmes-Déchaux 63040 Clermont-Ferrand Cedex 9, France*
(Dated: July 27, 2023)

ABSTRACT

Polymer nanocomposites (PNCs) are known to display exceptional non-linear mechanical properties, even for deformation amplitudes as low as a few percent. One of the most studied phenomenon is the so-called Payne effect, a drop in storage modulus with increasing amplitude. Several mechanisms have been put forward to rationalize such effect, including filler network breaking, polymer chain desorption and yielding of the polymer confined between the nanofillers. In this contribution, we demonstrate that for PNCs involving fractal-like aggregates, the Payne effect may originate from the alignment of the aggregates under the imposed flow direction. We reach this conclusion by using a coarse-grained model, which combines an explicit representation of fillers with an implicit description of the polymer matrix. We systematically characterize the effects of aggregate size and polydispersity in the amplitude of the Payne effect. Moreover, we probe the mechanical response of the model PNCs after a first cycle of deformation. We observe slow recovery kinetics of the original storage modulus of the PNCs and relate this memory effect to the alignment of the aggregates. Our findings should contribute to clarify the relation between the macroscopic mechanical response of the PNCs and the mesoscopic state of the filler.

I. INTRODUCTION

Dispersing a tiny amount of solid filler within a polymer matrix may change drastically the polymer rheology [1–3]. Pure polymer matrices exhibit a low plateau modulus and a linear response over a broad range of deformation amplitude. In contrast, polymer nanocomposites (PNCs) feature both a larger elastic modulus and even for small deformation amplitudes, strongly nonlinear effects. Prominent among them is the so-called Payne effect [4–12], which refers to the drop in storage modulus occuring for typical deformation amplitudes between 0.1 and 10%. Both the amplitude and the critical deformation amplitude depend on the nanofiller volume fraction. Alongside such nonlinear phenomena, it is well known that the rheology of PNCs may strongly depend on the mechanical history [13–15]: after a first deformation, PNCs do not recover instantaneously their original storage modulus.

The microscopic mechanism underlying the Payne effect is still being debated. A variety of hypotheses has been put forward, with at least four types of interpretations. A first class of model relates the Payne effect to polymer chains disentanglements under deformation [16, 17]. A second scenario posits that the drop in modulus is driven by polymer chains desorption or debonding, hence breaking the links of the percolating filler-network [11, 18–20]. Alternatively, the destruction of the filler network due to breaking of the solid aggregates or agglomerates is also invoked as a cause of stress softening [21–24]. Finally, it has been proposed that the Payne effect originates in the yielding of glassy bridges connecting neighbouring fillers [25–27]. In this latter case, the slow recovery kinetics after a first deformation is attributed to aging of the polymer confined between nanofillers.

To the question of the Payne effect origin, it is likely that there is not a single answer. The variety of available fillers continues to expand both in terms of shape and size [28, 29] and the resulting PNCs may differ considerably in properties. The relevance of each mechanism may depend on the particular system under investigation and on the experimental conditions. Moreover, given the complex physical chemistry PNCs, several mechanisms can compete and contribute concurrently to the Payne effect. The relevance of generic mechanisms can only be assessed on a specific system.

There are, however, several reasons to believe that a general scenario should be at work in the Payne effect. First, it has been long recognized, since the early investigations by Payne, that the drop of the elastic modulus is also observed in carbon black dispersed in a non-polymeric solvent [30]. Recent experimental studies confirm that carbon black suspensions in a silicon oil display a non-linear rheology phenomenology typical of filled elastomers [24, 31]. Two important implications follow as regards the possible physical interpretations of the Payne effect. On the one hand, chain entanglements can not explain the drop of the elastic modulus in the non polymeric systems, as the molecular weight of the silicon oils is less than the chain entanglement weight [31]. On the other hand, because rheological measurements are typically performed far above the silicon oil glass transition temperature, a glassy yielding mechanism is quite un-

* Corresponding authors: francois.detcheverry@univ-lyon1.fr, samy.merabia@univ-lyon1.fr

likely. Finally, another salient feature of the Payne effect is the wide temperature range over which it occurs [5, 32]. All these considerations point to a generic mechanism of the Payne effect, where the nanofiller aggregates play a dominant role and the matrix –whether polymeric or not– plays only a secondary role. In this article, we follow this line of thought and focus on the coupling between the aggregates and the imposed deformation to seek an interpretation of the Payne effect.

We focus specifically on polymer nanocomposites that involve fractal-like aggregates. Historically, the first widely studied PNCs were based on fractal-like aggregates made of carbon black. The interest in this type of fillers is related to the tire industry, which makes extensive use of carbon black fillers [2, 3]. More recently, silica nanoparticles either well dispersed or forming aggregates have been considered as alternative fillers [1]. Both carbon black and silica aggregates are made of hundreds of primary particles attached in a ramified structure which can reach 500 nm in size. Understanding their effect on viscoelastic and mechanical properties has been a long-standing quest [33–38].

While many puzzles remain in the understanding of PNCs [39], the large size of fractal-like aggregates poses a specific challenge. Simulation of polymeric materials have long offered a direct access to chain structure and dynamics [40, 41]. Yet, approaches based on a molecular description [19, 42, 43] or more coarse-grained models such as DPD or slip-links [44–46] are applicable only to PNCs with small fillers. They are difficult to exploit with fractal-like aggregates with typical size of 100 nm, because the relevant time and length scale remain mostly unaccessible. For this reason, we introduced in a previous work [47] a new mesoscopic model for fractal-like aggregate nanocomposites. Since polymeric chains are too costly to model explicitly, the matrix is described implicitly as a viscoelastic medium, in which interactinng aggregate particles, still represented explicitly, evolve through a generalized Langevin dynamics. Such a hybrid modeling makes it possible to simulate dozens of aggregates and to account for aggregate interactions, size and polydispersity. Within this framework, we previously investigated the viscoelastic properties of PNCs in the linear regime [47].

In this study, we use our implicit medium model for fractal aggregate nanocomposites to revisit the Payne effect. We first quantify how the size, volume fraction and polydispersity influence the amplitude of the phenomenon. Next, we show that the underlying microscopic mechanism involves the alignment of aggregates. Finally, we consider memory dependent effects arising in cycling protocols. The remainder of this article is structured as follows. In Sec. II, we briefly present the model for polymer and aggregates, the numerical method and choice of parameters. Section III is devoted to the results on Payne effect, orientation of aggregates and memory behavior. Section IV summarizes our findings.

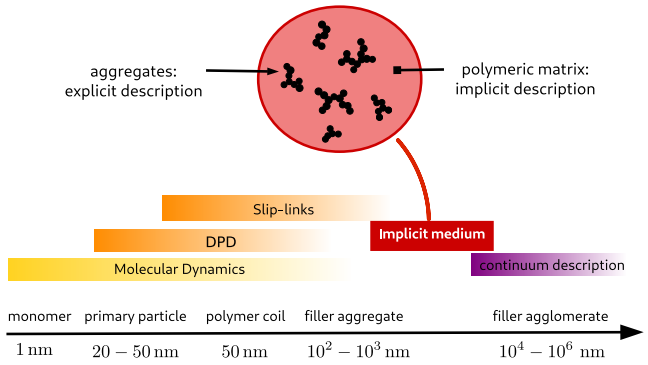

FIG. 1. **Implicit Medium Model.** The range of length scales accessible is approximately indicated for each numerical method.

II. MODEL AND METHOD

The simulation of polymer nanocomposites has been attacked through a variety of methods, which may be grouped in two classes (see Fig. 1). The first class relies on an explicit description of polymeric chains. Molecular dynamics [10, 41, 48, 49] can efficiently handle length scales that are characteristic of primary particles and polymer coil. More coarse-grained models such as slip-links [50, 51] or dissipative particle dynamics (DPD) [44, 52–54] give access to system an order of magnitude larger, reaching the size of a single aggregate. Yet, describing a large collection of aggregates – a requirement to understand their interaction and the effect of polydispersity – remains challenging. At the other end of the scale spectrum, the second type of approach treats the polymer nanocomposite as a continuum medium [55–58], where chain configurations and many aggregate features can not be accounted for. The implicit medium model seeks to address the gap in scale arising in between the class of explicit methods and the continuum approach. It is a hybrid approach that combines features from both classes: the polymer matrix is described implicitly as a continuum viscoelastic medium but the aggregates are still modelled explicitly in a particle-like description. Such a level of coarse-graining allows to simulate multi-aggregates systems.

To make the paper self-contained, we summarize below our implicit medium model of fractal-like PNCs. An exhaustive description, including a discussion of the underlying assumptions and details of the numerical method, can be found in Ref. [47].

A. Generalized Langeving Equation

Because aggregates are treated as collection of particles, it is sufficient to consider a single particle. Within the implicit medium model, its dynamics is governed by a generalized Langevin equation (GLE). For a particle

with mass m, position $\mathbf{r}$ and velocity $\mathbf{v}$, it reads as

$$m\frac{\mathrm{d}\mathbf{v}(t)}{\mathrm{d}t} = \mathbf{F}_\mathrm{c}\left(\mathbf{r}(t)\right) - \int_{-\infty}^{t} \Gamma(t-t')\mathbf{v}(t')\,\mathrm{d}t' + \mathbf{F}_\mathrm{r}(t). \quad (1)$$

Here, $\mathbf{F}_\mathrm{c}$ is the conservative force that describes interactions with other particles, specifically a steric repulsion as described by a truncated Lennard-Jones potential [47]. The effect of the surrounding medium is encapsulated in two distinct forces: a drag force $\mathbf{F}_\mathrm{d} = -\int_{-\infty}^{t}\Gamma(t-t')\mathbf{v}(t')\,\mathrm{d}t'$ that accounts for the average friction exerted by the matrix and a random force $\mathbf{F}_\mathrm{r}$ induced by thermal fluctuations. The memory kernel $\Gamma(t)$ involved in the drag force is related to the time correlation function of the random force through the fluctuation-dissipation theorem

$$\langle \mathbf{F}_\mathrm{r}(t)\,\mathbf{F}_\mathrm{r}(t')\rangle = k_\mathrm{B}T\,\Gamma(t-t')\boldsymbol{I}, \quad (2)$$

where k_B is Boltzmann's constant, T the temperature and $\boldsymbol{I}$ the identity matrix.

In our implicit description, the influence of the polymer matrix arises only through the memory kernel $\Gamma(t)$. The generalized Stokes law [59] and correspondence principle [60] indicate that the kernel $\Gamma(t)$ is proportional to the stress relaxation modulus $G_\mathrm{p}(t)$ of the medium:

$$\Gamma(t) = 6\pi R\,G_\mathrm{p}(t), \quad (3)$$

where we assume a a spherical particle of radius R and no-slip boundary condition at its surface. Throughout this study, we use the simplest model of viscoelastic medium, namely a Maxwell fluid whose stress relaxation modulus decays exponentially with a single relaxation time

$$G_\mathrm{p}(t) = G_\mathrm{p}^0 \exp\left(-\frac{t}{\tau_\mathrm{p}^0}\right), \quad (4)$$

with G_p^0 the plateau stress modulus and τ_p^0 the terminal relaxation time. Note that the method is nevertheless applicable to other matrix rheology. The only requirement is that the memory kernel $\Gamma(t)$ can be written as a Prony series, i.e. a sum of decaying exponentials, each with a given coefficent and relaxation time.

In contrast to traditional Brownian dynamics, the generalized Langevin equation involves both a correlated noise and a friction force that is non-local in time, because it depends on the whole history of velocity taken in the past. As a consequence, the simulation of Eq. (1) requires a specific numerical method. We use here the approach of Baczewski and Bond [61]. The principle is to introduce new variables to rewrite the non-Markovian GLE for particle motion as a Markovian evolution over an expanded state space. New degrees of freedom are thus necessary to describe the matrix behavior, but compared to the number of variables required for an explicit description of chains, their number is reduced by order of magnitudes. Therein lies the efficiency of the implicit medium approach.

B. Fractal-like aggregates

The solid fillers in our model are represented by groups of spherical particles whose spatial structure may be chosen at will. Those particles interact through the repulsive part of a truncated Lennard-Jones potential with energy ϵ and distance σ. As illustrated in Fig. 2, the aggregate shape is maintained by two types of springs. The connective springs link neighboring particles that are in contact. The virtual springs connect each particle to three other randomly chosen particles. The spring energy is $U_\mathrm{S}(r) = k/2(r-l_\mathrm{c})^2$, where the spring constant k is a constant but the rest length l_c depends on the particular spring considered. In addition to the repulsive interactions, the spring forces are the second contribution to the conservative term of Eq. (1). When the stiffness k is high enough, the combination of repulsion and spring networks is sufficient to maintain a quasi-rigid structure. The resulting rigid aggregates are the primary objects studied in this work. For comparison purpose, we will also briefly consider individual particles and flexible aggregates, wherein particles are linked through connective springs only. Note that, while breaking of aggregates may play a role in some real nanocomposites [62], here it is entirely discarded.

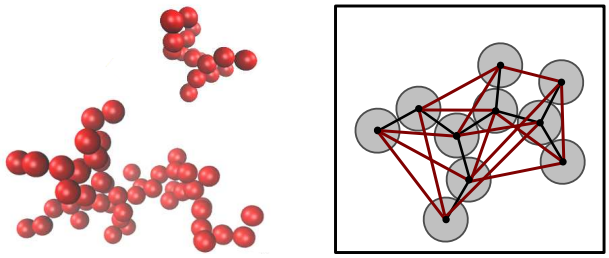

FIG. 2. **Model for fractal-like aggregates.** (Left) DLA-generated aggregate with size $\mathcal{N} = 20$ and 50. (Right) Model for rigid aggregates. Each particle is linked to its neighbors through connective springs (grey lines) and through three virtual springs (red lines), that maintain a quasi-rigid structure.

As a convenient approximation to aggregate fillers used in real PNCs, the aggregate morphology is generated by a diffusion-limited aggregation (DLA) process [63, 64]. Given their limited size, the resulting objects are not truly fractal but may be qualified as "fractal-like" because of their branched disordered structure. They can be characterized by the radius of gyration R_g and aspect ratio [47]. In the following, both monodisperse and polydisperse aggregates will be considered. Monodisperse aggregates have a fixed size $\mathcal{N}$, that is obtained by stopping the DLA process after $\mathcal{N}$ particles. Polydisperse aggregates are characterized by the probability distribution

$$P(\mathcal{N}) = \frac{\mathcal{N}^\alpha}{\Gamma(\alpha+1)\beta^{\alpha+1}} \exp\left(-\frac{\mathcal{N}}{\beta}\right), \quad (5)$$

with α and β parameters and Γ is the gamma function. We choose a most frequent aggregate size $\mathcal{N}_\mathrm{max} = \alpha\beta =$

20 and a mean $\langle \mathcal{N} \rangle = (\alpha + 1)\beta = 30$, resulting in a polydispersity around 30%. This choice is representative of the large polydispersity often observed in experimental systems [37].

C. Explicit shearing

In a previous study [47], we investigated the rheology of the PNCs in the linear regime. In that case, properties such as the stress relaxation modulus $G(t)$ are accessible via the linear response theory and Green-Kubo relation from the correlation function measured at equilibrium [65]. In contrast, we focus here on the non-linear regime and the non-equilibrium process by which shear flow is imposed needs to be simulated explicitly. To do so, together with Lees-Edwards boundary conditions [66], we use the SLLOD algorithm [67, 68]. Specifically, we assume a homogeneous shear flow $\mathbf{u}_{\text{ext}} = \dot{\gamma} y \mathbf{e}_x$, with $\dot{\gamma}$ a fixed shear rate. The velocity $\mathbf{v}$ of Eq. (1) is then the relative velocity between the particle and the polymer matrix. Note that when considering oscillatory shear imposed, it is assumed the linear velocity profile is established on a time scale shorter than all other processes.

Quantity	Symbol	Simulation	Real value
Energy	$k_{\text{B}}T$	1	$4.1\,10^{-21}$ J
Particle diameter	σ	1	9.4 nm
Polymer terminal time	τ_{p}^0	1	1 ms
Polymer plateau modulus	G_{p}^0	$100\,P_{\text{unit}}$	0.5 MPa

TABLE I. Choice of units and parameters for the typical polymer nanocomposite considered in simulation.

D. Parameters

Within the implicit model, it is natural to take the particle diameter σ as unit length, the polymer relaxation time τ_{p}^0 as unit time and $k_{\text{B}}T$ as unit energy. The polymer plateau modulus is set to $G_{\text{p}}^0 = 100 P_{\text{unit}}$, with $P_{\text{unit}} = k_{\text{B}}T/\sigma^3$ the unit pressure. Such a choice of parameters corresponds physically to a nanocomposite at room temperature, made of particles with diameter $\sigma = 9.4\,\text{nm}$, and dispersed in a polybutadiene matrix of molecular weight 40 K for which $G_{\text{p}}^0 = 0.5\,\text{MPa}$ and $\tau_{\text{p}}^0 = 1\,\text{ms}$ [69]. Table I collects the choice of units and default values. Other numerical parameters are similar to those of Ref. [47].

As regards the aggregates, the main physical parameters we focus on are the aggregate size $\mathcal{N}$, the monodisperse or polydisperse character and the volume fraction ϕ [70]. Results shown below are generated with systems containing typically 10^3 particles. With aggregate size $\mathcal{N}$ ranging between 20 and 50, this implies a number of aggregates N_{a} of a few dozens, which is sufficient to account for interactions between aggregates and polydispersity. An average over ten independent simulations was systematically taken to improve statistics.

E. Stress tensor

The main quantity of interest is the stress tensor

$$\sigma_{\alpha\beta} = -\frac{1}{V} \sum_{i<j} \langle F_{ij,\alpha} R_{ij,\beta} \rangle. \tag{6}$$

Here, α and β denote the x, y or z component, $\mathbf{F}_{ij}$ is the force applied by particle i on particle j, $\mathbf{R}_{ij}$ is the vector joining particle i to particle j, and indices i and j run over all particles in the system. We note that in this definition, only the contribution from the aggregates is taken into account. The contribution from the polymer matrix is constant, and for clarity of comparison, is not shown in what follows. If not mentioned otherwise, σ refers to the σ_{xy} component, with the x-axis in the direction of flow and the y-axis in the direction of shear.

III. RESULTS

A. Non-linear rheology

In the linear regime, the storage modulus G' and the loss modulus G'' may be obtained from a Fourier transform of the stress relaxation modulus $G(t)$ computed at equilibrium [71]. In the nonlinear regime [72–76], such a Green-Kubo approach is not valid any more and the dynamic moduli needs to be defined from the time relation between instantaneous stress and strain. Here we assume an oscillatory shear where the imposed deformation $\gamma(t)$ is sinusoidal with frequency ω and amplitude γ_0. The resulting stress $\sigma(t)$ involves only a phase difference in the linear regime but higher order harmonics in the non-linear regime:

$$\gamma(t) = \gamma_0 \sin(\omega t), \tag{7a}$$

$$\sigma(t) = \sum_{m \text{ odd}} \sigma_{m,0} \sin(m\omega t + \delta_m). \tag{7b}$$

Here γ_0 is the amplitude of shear deformation, $\sigma_{m,0}$ and δ_m are respectively the amplitudes and phase difference of shear stress at order m. The order number can only be odd because the stress response is assumed to be of odd symmetry [73, 74, 76]. The nonlinear regime is entered when harmonic terms whith $m > 1$ can not be neglected. In practice, for all results shown below the amplitudes $\sigma_{m,0}$ and phase differences δ_m are obtained by a fit of the stress by Eq. (7b), where the sum is restricted to three terms $m = 1$, 3 and 5. The storage and the loss modulus of order m, G'_m and G''_m respectively, can then

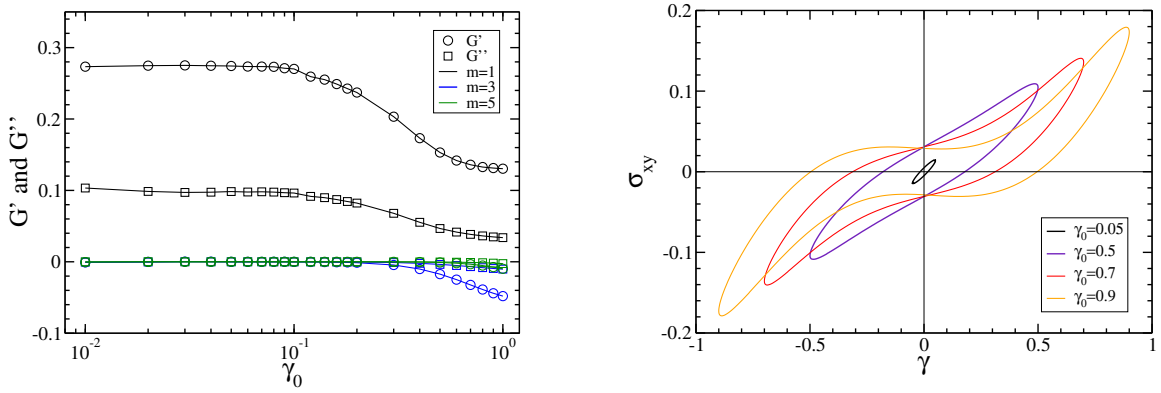

FIG. 3. **Non-linear effects** (Left) Order m component of the storage and loss moduli G' and G''. Note that the vertical axis is not logarithmic but linear. (Right) Lissajous figure: stress as a function of strain for various deformation amplitudes. The system parameters are: $\mathcal{N} = 20$ and $\phi = 10\%$.

be calculated from

$$G'_m(\omega) = \frac{\sigma_{m,0}}{\gamma_0} \cos\delta_m, \tag{8a}$$

$$G''_m(\omega) = \frac{\sigma_{m,0}}{\gamma_0} \sin\delta_m. \tag{8b}$$

The loss factors δ_m, defined from $\tan\delta_m = G''_m/G'_m$, may also be used to quantify the elastic or viscous nature of system response. From now on, we fix the frequency of oscillations to $\omega = 1$ in units of $1/\tau_{\rm p}^0$, a value lying in the lower part of the frequency spectrum, of order 10^3 Hz.

B. Payne effect

Figure 3 shows the dynamic moduli of a weakly reinforced system as a function of the strain amplitude. Two features needs to be highlighted. First, both storage and loss moduli drop for strain amplitudes $\gamma_0 \geq 0.2$. Second, the linear term ($m = 1$ in Eq. (8a)) is completely dominant up to $\gamma_0 \geq 0.2$. Above this value, which signals the beginning of the nonlinear regime, the next harmonic $m = 3$ becomes significant, with an amplitude that is almost one-half of the primary term when $\gamma_0 \simeq 1$. Alternatively, the non-linearity of the PNC elastic response can be made apparent with a Lissajous figure. As shown in Fig. 3.right, the instantaneous stress is plotted as a function of the shear deformation. At small deformation amplitude γ_0, the curve is perfectly elliptical because strain and stress differ only by a phase difference, indicative of a perfect viscoelastic behavior. In contrast, at large amplitude, the curve develops an inverted sigmoidal shape with pronounced horns, a departure from elliptic shape that is characteristic of non-linearity. Note that the area enclosed by the Lissajous curve is the average energy dissipated per unit volume and per cycle. Though the higher harmonics are not negligible, we focus, in the following, for simplicity on the primary term $m = 1$. The storage and the loss moduli plotted below correspond to G'_1 and G''_1, if not mentioned otherwise.

We investigate now how the amplitude of the Payne effect depends on the microscopic parameters characterizing the aggregates. Figure 4 compares the storage and loss moduli of flexible and rigid fractal aggregates PNCs. Two preliminary remarks are in order. First, we note that in the linear regime ($\gamma_0 < 0.1$), the results obtained with the non-equilibrium oscillatory shear imposed with SLLOD are similar to those obtained previously using Green-Kubo relation and equilibrium simulations [47]. Such an agreement between two different techniques confirms the consistency of the approach. Second, both flexible and rigid aggregates induce an increase in dynamic moduli G' and G'', with an enhancement in amplitude of one order and two orders of magnitude respectively. Because of the weak volume fraction of filler considered here ($\phi = 10\%$), the reinforcement factor remains relatively moderate but is known to increase at higher volume fraction [47].

For all systems and conditions explored, we observe a reduction of storage and the loss moduli at large deformation amplitude (Fig. 4.left), in agreement with the typical phenomenology observed in PNCs [1]. This suggests that only minimal ingredients – repulsive aggregates in a viscous matrix – are needed to generate a Payne effect, which therefore can be expected on a generic basis. This observation is also consistent with recent experimental investigations which show evidence of a large drop of the elastic modulus in carbon black aggregates dispersed in oil [24]. In the next section, we will interpret this phenomenon by looking at the change of orientation of the aggregates during shear flow. Before doing so, we characterize the Payne effect in our model fractal aggregate PNCs, by showing its dependence on the aggregates properties: filler type, aggregate size, polydispersity and volume fraction.

The Payne effect is partly influenced by the type of filler. The main difference is the reduction factor of G' that is higher for rigid aggregates. The reduction factor of G'' is quite similar, around a factor 3 within the range of shear amplitude explored. From now on, we fo-

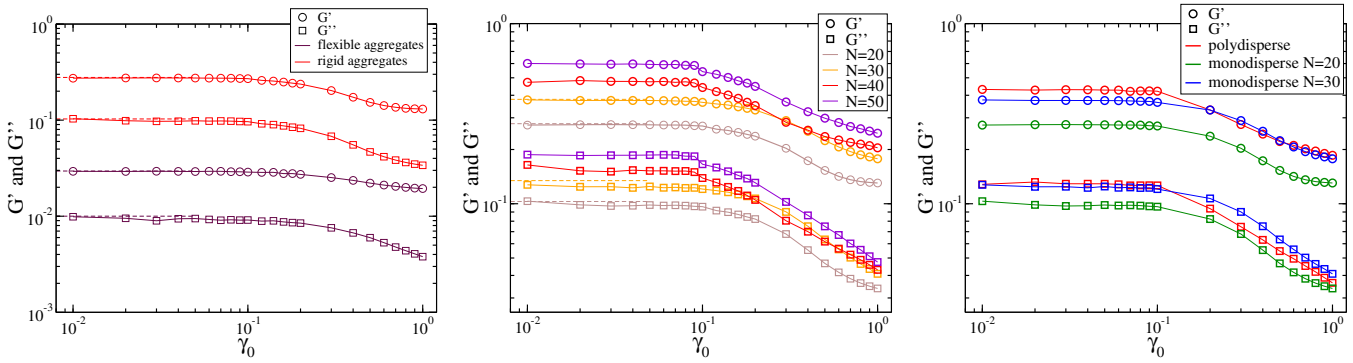

FIG. 4. **Influence of aggregate properties on Payne effect.** (Left) Effect of the filler type: flexible and rigid aggregates ($\mathcal{N} = 20$ and $\phi = 10\%$). The dashed lined indicates the modulus value obtained in the linear regime with a Green-Kubo method. (Middle) Effect of the aggregate size $\mathcal{N} = 20$ to 50 and $\phi = 10\%$. Dashed lines as above. (Right) Effect of polydispersity of aggregates. The polydisperse system is compared to monodisperse systems with $\mathcal{N} = 20$ and 30 ($\phi = 10\%$).

cus on the rigid aggregates because they represent the most interesting and realistic case. The influence of aggregate size is shown in Fig. 4.middle. For monodisperse aggregates with a fixed volume fraction $\phi = 10\%$, the aggregate size is increased from $\mathcal{N} = 20$ to 50. The general effect on the moduli is a shift to higher values, up to a threefold increase, but leaving the curve aspect mostly unchanged. In particular, the values of the dynamic moduli found at the largest deformation probed ($\gamma_0 = 1$) are always nearly $2-3$ times smaller than those found in the linear regime. This implies that in relative terms, the amplitude of the Payne effect is independent of the aggregate size.

The effect of polydispersity is illustrated in Fig. 4.right. For comparison, we also plot the result for two monodisperse systems with sizes $\mathcal{N} = 20$ and 30, which are respectively the most frequent size and the mean size of the polydisperse system. The polydisperse curve is not a simple reweighting of the monodisperse curves. In particular, the storage modulus is higher in the linear regime, and very close to the $\mathcal{N} = 30$ curve in the nonlinear regime. This suggests that the largest aggregates with size exceeding $\mathcal{N} = 30$ that may be present in the polydisperse system yields a significant contribution to the storage modulus, in spite of their small number. On the other hand, for the loss modulus in the non-linear regime, the polydisperse curve does lie in between the two monodisperse curves. Overall, this indicates that a polydisperse system can not be understood as superposition of monodisperse systems but involves specific effects between aggregates of different sizes.

Finally, the Payne effect appears to have a simple dependence on volume fraction, as illustrated in Fig. SM1 of Supplementary Material (SM). Increasing ϕ from 10% to 15% only results in an overall shift of the moduli curves. Note however that, because of the challenge in generating configurations of rigid aggregates, in particular for the monodisperse system [47], this observation holds only for the moderate volume fraction that could be tested and that the behavior may be different at higher volume fraction.

C. Aggregate orientation

We now seek a microscopic interpretation of the Payne effect in our model of fractal aggregates polymer nanocomposite. In contrast to what happens at equilibrium, the aggregates simulated under explicit shear are subject to a finite deformation that may alter their shape and orientation. To quantify the phenomenon and assess its role in the Payne effect, we characterize the aggregate conformation by using the gyration tensor [77]

$$\overline{\overline{S}} = \frac{1}{\mathcal{N}} \sum_{n=1}^{\mathcal{N}} \mathbf{x}_n \mathbf{x}_n^T, \tag{9}$$

where $\mathbf{x}_n^T$ is the transpose of $\mathbf{x}_n = \mathbf{r}_n - \mathbf{r}_{\rm cm}$, $\mathbf{r}_n$ the position of the $n^{\rm th}$ particle and $\mathbf{r}_{\rm cm}$ the position of the center of mass. As a real symmetric matrix, $\overline{\overline{S}}$ can be diagonalized and the eigenvalues $\lambda_1 > \lambda_2 > \lambda_3$ and eigenvectors define respectively the extent and orientation of the corresponding ellipsoid. Because the distribution of aspect ratio $\kappa = \lambda_1/\lambda_3$ deviates significantly from unity [47], it is meaningful to associate to each aggregate the orientation of its principal axis. In practice, this definition must be slightly amended. Because the aggregates are not strictly rigid but can slightly deform, the largest eigenvalue may switch from one axis to the other between two successive time steps. In that case, we choose the eigenvector in the current step which has maximum overlap with the eigenvector in the previous step. In this way, jumps in orientation are avoided and the orientation and main axis of all aggregates evolve continuously. It is also convenient to introduce an orientation angle θ, as shown in Fig. 5.left. With the matrix velocity along $\mathbf{e}_x$ and the shear along $\mathbf{e}_y$, θ denotes the angle between $\mathbf{e}_x$ and the projection of the main axis in the $x-y$ plane.

To quantify any ordering trend in aggregates, we considered $P(\cos\theta)$, the distribution of orientation angle co-

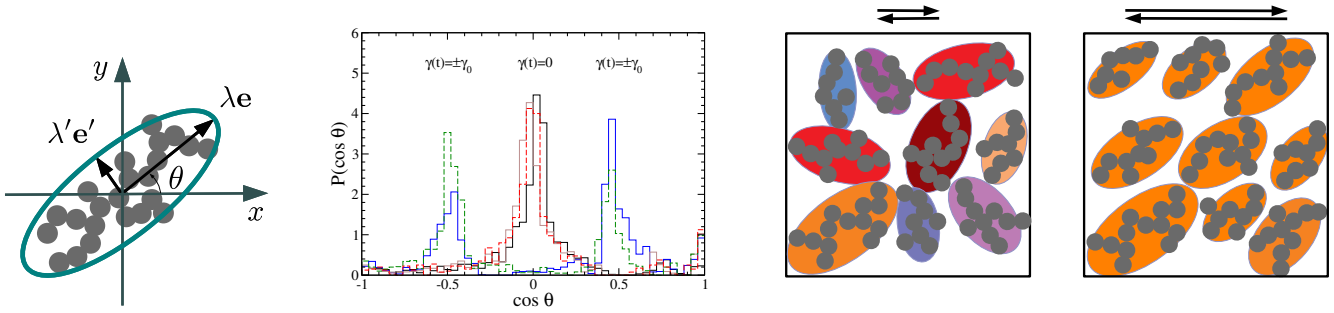

FIG. 5. **Orientation of aggregates at high shear amplitude.** (Left) Two-dimensional schematic of the aggregate orientation θ: each aggregate is assimilated to an ellipsoid whose main axis is along the unit vector $\mathbf{e}$. (Middle) Density probability of orientation angle at various time points under large shear deformation ($\gamma_0 = 0.5$). System parameters are: $\mathcal{N} = 20$ and $\phi = 10\%$, as in Fig. 3. (Right) Schematic of the aggregate orientation at small and large shear amplitude. At low γ_0, the distribution of the orientation of the aggregates is isotropic. By contrast, at high γ_0, the aggregates tend to align with each other.

sine, computed at different times throughout the shear oscillation period and averaged over all periods in steady state. In the linear regime ($\gamma_0 = 0.1$, not shown), there is no recognizable trend in $P(\cos\theta)$, suggesting an isotropic orientation of aggregates that is consistent with their initial state. In contrast, in the nonlinear regime ($\gamma_0 = 0.5$), the distribution $P(\cos\theta)$ is strongly peaked at a position that depends on the time considered, as can be seen in Fig. 5.middle. In particular, when the instantaneous deformation is extremal (time points where $\gamma(t) = \pm\gamma_0$), the aggregates tend to align along the principal shear directions ($\theta = \pm\pi/4$). Large amplitude shear deformation does affect the orientation of aggregates and the steady state they reach is different from the initial equilibrium state that was isotropic.

Schematically, the simulation data suggests the following picture (Fig. 5.right): while aggregates orientation in the linear regime is unbiased, aggregates in the nonlinear regime tend to align with each other and rotate simultaneously. At the extreme points of the shear cycle ($\gamma(t) = \pm\gamma_0$), when shear reverses direction, the aggregates align with the principal shear direction. Since the phenomenon occurs simultaneously with the Payne effect, it appears as one underlying mechanism. Indeed, alignment of aggregates reduce repulsive interactions between them, and presumably the ability to resist deformation, hence the drop in moduli. We have found this simple picture to apply equally in monodisperse and polydisperse systems, and conclude that it plays a significant role in the Payne effect of our implicit medium model.

As a side remark, we note that the rigid aggregates considered here are unbreakable and quite resistant to deformation. A quantitative measure of deformation may be given by the ratio $\upsilon = \lambda_1(t)/\lambda_1(t=0)$ between the instantaneous largest eigenvalue $\lambda_1(t)$ and its initial value. At equilibrium and in the linear regime, the probability distribution $P(\upsilon)$ is peaked around unity, with deviation above 10% that are negligible. Under large deformation, larger deviation, up to 20%, may happen. However, overall, the deformation of aggregates remains limited and the main effect appears to lie in their orientation.

D. Memory-dependent rheological behavior

We now explore the consequences of the alignment of the aggregates on the memory dependent rheological behavior of the PNCs systems. Having shown that large amplitude oscillations induce an orientation ordering of aggregates, we are lead to the question: does the biased orientation of aggregates survive when reducing the amplitude or does the system lose memory of its partial ordering? The system is now submitted to a non trivial deformation history, as shown in Fig. 6.left. Using step-wise change of 10%, the deformation amplitude is first increased from $\gamma_0 = 0.1$ to 1 then decreased back to 0.1, thus defining the loading branch and the unloading branch of a cycle. For every value of γ_0, the system is left for more than 600 oscillation periods, a time generally sufficient to reach a steady state and record the dynamic moduli.

Shown in Fig. 6.middle are the results for polydisperse aggregates with volume fraction $\phi = 10\%$. While the storage and the loss moduli exhibit a monotonous decrease during the loading process, they do not trace back their initial path during the unloading process, but define a clearly distinct branch. Compared to the initial state, the final state has moduli approximately 30% lower. The difference is also visible in the time-dependence of the stress $\sigma(t)$ averaged over successive periods (Fig. 6.right). At high amplitude $\gamma_0 = 0.5$, the stress signal, though clearly involving higher harmonics, is almost identical in the loading and unloading branches. At low amplitude $\gamma_0 = 0.1$, the stress, though sinusoidal in both branches, is significantly reduced in the unloading process.

If the final state after one cycle is different from the initial state, it is nonetheless conceivable that given sufficient time, the system would eventually relax toward the initial state. This hypothesis was tested with simula-

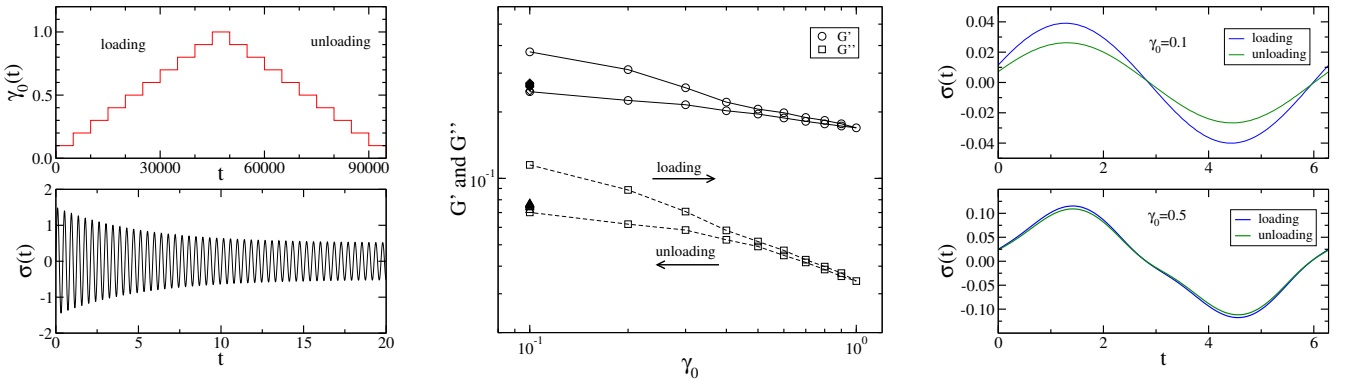

FIG. 6. **Memory-dependent rheology with one cycle.** (Left) Schematic of the loading-unloading process. The amplitude $\gamma_0(t)$ is changed stepwise and the stress $\sigma(t)$ oscillations relax toward a steady state amplitude. (Middle) Moduli G' and G'' during the loading-unloading process. Aggregates are polydisperse and $\phi = 10\%$. (Right) Average shear stress over one period in steady state in the loading and the unloading processes at deformation amplitude $\gamma_0 = 0.1$ (top) and $\gamma_0 = 0.5$ (bottom).

tions ten times longer than the usual duration, and that include 6000 cycles, while keeping the deformation amplitude fixed to $\gamma_0 = 0.1$. Both the mono- and the polydisperse aggregate systems display very little evolution in their storage and loss moduli. This suggests that the oriented stationary state induced by large shear deformation persists and that the system remains "locked" at least over time scales accessible in our simulations (typically 1 s).

To further assess the memory effects, we finally consider multiple cycles, with a series of three cycles of loading-unloading process. The result shown in Fig. 7 for polydisperse aggregates at $\phi = 17\%$ is representative of the behavior seen in systems with different size distribution or volume fraction. It appears that the initial state is never recovered. Rather, the second and third cycles entirely overlap with the unloading branch of the first cycle, suggesting that the memory of orientational ordering is maintained throughout. To confirm this interpretation, we have examined the distribution of orientation angles, which show no drastic evolution after the first cycle [78]. To get a quantitative measure, we use the nematic order parameter

$$\zeta = 2\langle \cos^2 \theta \rangle - 1, \tag{10}$$

where $\langle ... \rangle$ denotes an ensemble average, taken at the extreme points of the shear cycle (where $\gamma(t) = \pm\gamma_0$). As shown in the inset of Fig. 7, the orientational order is strongly enhanced after the first cycle, but show a much weaker evolution, if any, in the two subsequent cycles. It thus appears that aggregates are oriented at high deformation amplitude during the loading process of the first cycle, and essentially maintain their ordered state afterwards. This points to a memory effect relating the microscopic state of aggregates and the macroscopic rheological properties of the nanocomposites.

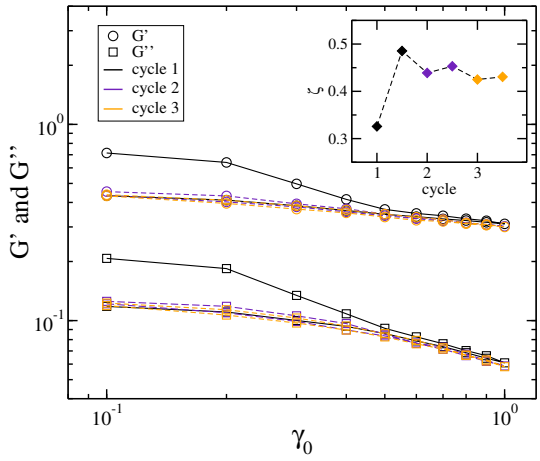

FIG. 7. **Memory-dependent effect: three cycles.** Storage and loss modulus along three cycles of shear deformation amplitude. Aggregates are polydisperse and $\phi = 17\%$. (Inset) Nematic order parameter ζ of Eq. (10).

IV. CONCLUSION

To summarize, we explored here the non-linear mechanical behavior of a simple model of fractal aggregates dispersed in a viscoelastic matrix. We found a phenomenology typical of real PNCs, in particularly the drop of the elastic modulus for strain amplitudes on the order of 10%. Additionaly, we saw that the non-linearity of the stress response is dominated by the first term ($m = 1$ in Eq. 8a) and higher non-linear terms with $m \geq 3$ are subdominant. We also investigated the effects of the aggregate size and polydispersity in the drop of the elastic modulus.

We related the existence of a Payne effect in our system to a collective alignement of aggregates. At low shear amplitude ($\gamma < 0.1$), the distribution of aggregate orientation is isotropic. The shear flow does not perturb

strongly such initial state and one finds a relatively high value of the storage modulus. By contrast, when the shear amplitude is larger, $\gamma_0 > 0.5$, the elastic modulus which measures the stress response of the system decreases, because the aggregates are oriented by the shear flow (Fig. 5).

At high filler volume fractions, the collective orientation of the aggregates should have even more drastic influence on the modulus drop. In the absence of deformation, or for low deformation amplitude γ_0, the system should be in a jammed state, as steric interactions between the aggregates severely hinder their mobility, and the elastic modulus should be relatively high. This scenario is consistent with a recent theoretical picture [79]. When deformed sufficiently, aggregate alignement reduces the number of contacts between aggregates, and presumably the ability to resist deformation, hence the drop in moduli. Our observations are also reminiscent of shear-induced alignement of anisotropic particles reported in granular and colloidal systems [80–82], and more generally of self-organization of periodically sheared particle suspensions [83]. Whether a precise analogy can be established remains to be investigated and deserves a devoted study.

The interpretation we propose is rather generic and should be at play in any composite system made of fractal or loose aggregates. In particular, our implicit medium model accounts neither for polymer chain bonding nor for glassy layers which may surround the nanoparticles. From this perspective, our interpretation is in line with recent experimental findings [24] and early experimental investigations of Payne [30, 84], which both reported a large drop modulus for dispersions of carbon black aggregates in oil. In such a system, polymer bonding, entanglements or glassy layers are quite unlikely, they nonetheless display a Payne effect typical of PNCs. That being said, we expect our interpretation to be equally relevant for polymeric systems. In many PNCs, the shear orientation of the aggregates - whether fractal or not- is potentially a key phenomenon and should compete with other mechanisms depending on temperature or the physical chemistry features of the systems considered.

We also highlighted the role of the aggregate orientation in the memory effects of the elastic moduli. First, large deformations change the orientation state of aggregates, with a collective alignment that persists for a significant time thereafter. This results in stress-strain curves that depend on the mechanical history of the system, and a relative stress softening of the system. Our simulations show that these effects persist for times much longer than the matrix terminal relaxation time. Indeed, due to the steric constraints between the aggregates, the return back to the initial state of isotropically-distributed aggregates, is a rather slow process, as revealed by the time evolution of the nematic order parameter.

Our aim in this study was to propose a microscopic interpretation of the Payne effect in a simple model of fractal aggregate polymer nanocomposites, in order to disentangle several possible causes of this effect. Yet, starting from the present description, several directions may be pursued to seek an improved modeling of real PNCs. The first deals with interaction between aggregates. They were supposed purely repulsive here, which is sufficient to avoid any overlap during shear deformation. But the interaction between real aggregates could be attractive at large distances, either because of long range van der Waals interactions or to take into account in an effective manner the possible polymer chain bonding between neighbouring nanoparticles. Preliminary results show that an attractive interaction between aggregates has a significant effect on the loss properties of the system, which deserves to be studied exhaustively. Another perspective is to adopt a realistic modeling of the viscoelastic properties of the matrix, in both the linear and non-linear regimes of deformation.

REFERENCES

[1] Vilgis, T. A., Heinrich, G., Klüpell, M., Kluepell, M., *Reinforcement of Polymer Nano-Composites: Theory, Experiments and Applications*, (Cambridge University Press 2009).

[2] Nielsen, L., Landel, R., *Mechanical properties of polymers and composites*, (Dekker, New York 1994).

[3] Mark, J. E., Erman, B., Eirich, F., *The Science and Technology of Rubber*, (Academic Press, San Diego 1994).

[4] Fletcher, W. P., Gent, A. N., Nonlinearity in the Dynamic Properties of Vulcanized Rubber Compounds. *Rubber Chem. Technol.* **27**, 209 (1954).

[5] Payne, A., The dynamic properties of carbon black loaded natural rubber vulcanizates. Part I. *J. Appl. Polym. Sci.* **6**, 57 (1962).

[6] Chazeau, L., Brown, J. D., Yanyo, L. C., Sternstein, S. S., Modulus recovery kinetics and other insights into the Payne effect for filled elastomers. *Polym. Compos.* **21**, 202 (2000).

[7] Cassagnau, P., Payne effect and shear elasticity of silica-filled polymers in concentrated solutions and in molten state. *Polymer* **44**, 2455 (2003).

[8] Gusev, A. A., Micromechanical mechanism of reinforcement and losses in filled rubbers. *Macromolecules* **39**, 5960 (2006).

[9] Ramier, J., Gauthier, C., Chazeau, L., Stelandre, L., Guy, L., Payne effect in silica- filled styrene–butadiene rubber: Influence of surface treatment. *J. Polym. Sci., Part B: Polym. Phys.* **45**, 286 (2007).

[10] Allegra, G., Raos, G., Vacatello, M., Theories and simulations of polymer-based nanocomposites: From chain statistics to reinforcement. *Prog. Polym. Sci.* **33**, 683 (2008).

[11] Moll, J. F., Akcora, P., Rungta, A., Gong, S., Colby, R. H., Benicewicz, B. C., Kumar, S. K., Mechanical re-

inforcement in polymer melts filled with polymer grafted nanoparticles. *Macromolecules* **44**, 7473 (2011).
[12] Gan, S., Wu, Z. L., Xu, H., Song, Y., Zheng, Q., Viscoelastic Behaviors of Carbon Black Gel Extracted from Highly Filled Natural Rubber Compounds: Insights into the Payne Effect. *Macromolecules* **49**, 1454 (2016).
[13] Mullins, L., Effect of Stretching on the Properties of Rubber (1948).
[14] Medalia, A. I., Elastic Modulus of Vulcanizates As Related To Carbon Black Structure. *Rubber Chem. Technol.* **46**, 877 (1973).
[15] Donnet, J.-B., Chand, R., Meng, B., editors, *Carbon Black*, (CRC Press 1993).
[16] Jouault, N., Dalmas, F., Boué, F., Jestin, J., Multiscale characterization of filler dispersion and origins of mechanical reinforcement in model nanocomposites. *Polymer* **53**, 761 (2012).
[17] Sternstein, S. S., Zhu, A. J., Reinforcement mechanism of nanofilled polymer melts as elucidated by nonlinear viscoelastic behavior. *Macromolecules* **35**, 7262 (2002).
[18] Thomin, J. D., Keblinski, P., Kumar, S. K., Network Effects on the Nonlinear Rheology of Polymer Nanocomposites. *Macromolecules* **41**, 5988 (2008).
[19] Sen, S., Thomin, J. J., Kumar, S., Keblinski, P., Molecular underpinnings of the mechanical reinforcement in polymer nanocomposites. *Macromolecules* **40**, 4059 (2007).
[20] Akcora, P., Kumar, S. K., Moll, J., Lewis, S., Schadler, L. S., Li, Y., Benicewicz, B. C., Sandy, A., Narayanan, S., Ilavsky, J., Thiyagarajan, P., Colby, R. H., Douglas, J. F., "Gel-like" Mechanical Reinforcement in Polymer Nanocomposite Melts. *Macromolecules* **43**, 1003 (2010).
[21] Kraus, G., Mechanical losses in carbon-black-filled rubbers. *Appl. Polym. Symp.* **39**, 1984 (1984).
[22] Maier, P. G., Göritz, D., Molecular interpretation of the Payne effect. *KGK, Kautsch. Gummi Kunstst.* **49**, 18 (1996).
[23] Hentschke, R., The Payne effect revisited. *EXPRESS Polym. Lett.* **11**, 278 (2017).
[24] Warasitthinon, N., Genix, A. C., Sztucki, M., Oberdisse, J., Robertson, C. G., The Payne effect: Primarily polymer-related or filler-related phenomenon? *Rubber Chem. Technol.* **92**, 599 (2019).
[25] Berriot, J., Montes, H., Lequeux, F., Long, D., Sotta, P., Gradient of glass transition temperature in filled elastomers. *Europhys. Lett.* **64**, 50 (2003).
[26] Montes, H., Lequeux, F., Berriot, J., Influence of the Glass Transition Temperature Gradient on the Nonlinear Viscoelastic Behavior in Reinforced Elastomers. *Macromolecules* **36**, 8107 (2003).
[27] Merabia, S., Sotta, P., Long, D. R., A Microscopic Model for the Reinforcement and the Nonlinear Behavior of Filled Elastomers and Thermoplastic Elastomers (Payne and Mullins Effects). *Macromolecules* **41**, 8252 (2008).
[28] Winey, K., Vaia, R., Polymer nanocomposites. *MRS Bulletin* **32**, 314 (2007).
[29] Kumar, S. K., Benicewicz, B. C., Vaia, R. A., Winey, K. I., 50th Anniversary Perspective: Are Polymer Nanocomposites Practical for Applications? *Macromolecules* **50**, 714 (2017).
[30] Payne, A., Study of carbon black structures in rubber. *Rubber Chem. Technol.* **38**, 387 (1965).
[31] Kawaguchi, M., Okuno, M., Kato, T., Rheological properties of carbon black suspensions in a silicone oil. *Langmuir* **17**, 6041 (2001).
[32] Clément, F., Bokobza, L., Monnerie, L., Investigation of the Payne effect and its temperature dependence on silica-filled polydimethylsiloxane networks. Part I: Experimental results. *Rubber Chem. Technol.* **78**, 211 (2005).
[33] Khan, S. A., Zoeller, N. J., Dynamic rheological behavior of flocculated fumed silica suspensions. *J. Rheol.* **37**, 1225 (1993).
[34] Mélé, P., Marceau, S., Brown, D., De Puydt, Y., Albérola, N. D., Reinforcement effects in fractal-structure-filled rubber. *Polymer* **43**, 5577 (2002).
[35] Jouault, N., Vallat, P., Dalmas, F., Jestin, J., Well dispersed fractal aggregates as filler in polymer- silica nanocomposites : long range effects in rheology. *Macromolecules* **42**, 2031 (2009).
[36] Kumar, S. K., Krishnamoorti, R., Nanocomposites: structure, phase behavior, and properties. *Annu. Rev. Chem. Biomol. Eng.* **1**, 37 (2010).
[37] Baeza, G. P., Genix, A. C., Degrandcourt, C., Petitjean, L., Gummel, J., Couty, M., Oberdisse, J., Multiscale filler structure in simplified industrial nanocomposite silica/SBR systems studied by SAXS and TEM. *Macromolecules* **46**, 317 (2013).
[38] Cassagnau, P., Linear viscoelasticity and dynamics of suspensions and molten polymers filled with nanoparticles of different aspect ratios. *Polymer* **54**, 4762 (2013).
[39] Kumar, S. K., Ganesan, V., Riggleman, R. A., Perspective: Outstanding theoretical questions in polymer-nanoparticle hybrids. *J. Chem. Phys.* **147**, 020901 (2017).
[40] Jancar, J., Douglas, J., Starr, F., Kumar, S., Cassagnau, P., Lesser, A., Sternstein, S., Buehler, M., Current issues in research on structure–property relationships in polymer nanocomposites. *Polymer* **51**, 3321 (2010).
[41] Vogiatzis, G. G., Theodorou, D. N., Multiscale Molecular Simulations of Polymer-Matrix Nanocomposites. *Arch. Computat. Methods. Eng.* **25**, 591 (2018).
[42] Pandey, Y. N., Papakonstantopoulos, G. J., Doxastakis, M., Polymer/Nanoparticle Interactions: Bridging the Gap. *Macromolecules* **46**, 5097 (2013).
[43] Hagita, K., Morita, H., Doi, M., Takano, H., Coarse-Grained Molecular Dynamics Simulation of Filled Polymer Nanocomposites under Uniaxial Elongation. *Macromolecules* **49**, 1972 (2016).
[44] Lahmar, F., Tzoumanekas, C., Theodorou, D. N., Rousseau, B., Onset of entanglements revisited. Dynamical analysis. *Macromolecules* **42**, 7485 (2009).
[45] Tzoumanekas, C., Lahmar, F., Rousseau, B., Theodorou, D. N., Onset of Entanglements Revisited. Topological Analysis. *Macromolecules* **42**, 7474 (2009).
[46] Masnada, E., Merabia, S., Couty, M., Barrat, J. J.-L. J., Entanglement-induced reinforcement in polymer nanocomposites. *Soft Matter* **9**, 10532 (2013).
[47] Wang, Y., Maurel, G., Couty, M., Detcheverry, F., Merabia, S., Implicit Medium Model for Fractal Aggregate Polymer Nanocomposites: Linear Viscoelastic Properties. *Macromolecules* **52**, 2021 (2019).
[48] Wang, L., Zheng, Z., Davris, T., Li, F., Liu, J., Wu, Y., Zhang, L., Lyulin, A. V., Influence of Morphology on the Mechanical Properties of Polymer Nanocomposites Filled with Uniform or Patchy Nanoparticles. *Langmuir* **32**, 8473 (2016).
[49] Behbahani, A. F., Rissanou, A., Kritikos, G., Doxastakis, M., Burkhart, C., Polińska, P., Harmandaris, V. A.,

Conformations and Dynamics of Polymer Chains in Cis and Trans Polybutadiene/Silica Nanocomposites through Atomistic Simulations: From the Unentangled to the Entangled Regime. *Macromolecules* **53**, 6173 (2020).

[50] Tzoumanekas, C., Theodorou, D. N., From atomistic simulations to slip-link models of entangled polymer melts: Hierarchical strategies for the prediction of rheological properties. *Curr. Opin. Solid State Mater. Sci.* **10**, 61 (2006).

[51] Biondo, D. D., Masnada, E. M., Merabia, S., Couty, M., Barrat, J.-L., Numerical study of a slip-link model for polymer melts and nanocomposites. *J. Chem. Phys.* **138**, 194902 (2013).

[52] Groot, R. D., Warren, P. B., Dissipative particle dynamics: Bridging the gap between atomistic and mesoscopic simulation. *J. Chem. Phys.* **107**, 4423 (1997).

[53] Masubuchi, Y., Langeloth, M., Böhm, M. C., Inoue, T., Müller-Plathe, F., A Multichain Slip-Spring Dissipative Particle Dynamics Simulation Method for Entangled Polymer Solutions. *Macromolecules* **49**, 9186 (2016).

[54] Kempfer, K., Devémy, J., Dequidt, A., Couty, M., Malfreyt, P., Multi-scale modeling of the polymer-filler interaction. *Soft Matter* **16**, 1538 (2020).

[55] Smallwood, H. M., Limiting law of the reinforcement of rubber. *J. Appl. Phys.* **15**, 758 (1944).

[56] Christensen, R. M., *Mechanics of Composite Materials*, (Dover 2005).

[57] Huber, G., Vilgis, T. A., On the mechanism of hydrodynamic reinforcement in elastic composites. *Macromolecules* **35**, 9204 (2002).

[58] Torquato, S., *Random heterogeneous materials*, (Springer, New York 2002).

[59] MacKintosh, F. C. C., Schmidt, C. F. F., Microrheology. *Curr. Opin. Colloid Interface Sci.* **4**, 300 (1999).

[60] Indei, T., Schieber, J. D., Córdoba, A., Pilyugina, E., Treating inertia in passive microbead rheology. *Phys. Rev. E* **85**, 021504 (2012).

[61] Baczewski, A. D., Bond, S. D., Numerical integration of the extended variable generalized Langevin equation with a positive Prony representable memory kernel. *J. Chem. Phys.* **139**, 044107 (2013).

[62] Asylbekov, E., Trunk, R., Krause, M. J., Nirschl, H., Microscale Discrete Element Method Simulation of the Carbon Black Aggregate Fracture Behavior in a Simple Shear Flow. *Energy Technology* **9**, 2000850 (2021).

[63] Sander, L. M., Diffusion-limited aggregation: a kinetic critical phenomenon? *Contemp. Phys.* **41**, 203 (2000).

[64] Seager, C. R., Mason, T. G., Slippery diffusion-limited aggregation. *Phys. Rev. E* **75**, 011406 (2007).

[65] Chandler, D., *Introduction to modern statistical mechanics*, (Oxford University Press 1987).

[66] Allen, M. P., Tildesley, D. J., *Computer Simulation of Liquids*, (Oxford University Press 1989).

[67] Evans, D. J., Morriss, G. P., *Statistical Mechanics of Nonequilibrium Liquids*, (Cambridge University Press 2008).

[68] Evans, D. J., Morriss, O. P., Non-Newtonian molecular dynamics. *Comput. Phys. Rep.* **1**, 297 (1984).

[69] Zhu, Z., Thompson, T., Wang, S.-Q., von Meerwall, E. D., Halasa, A., Investigating Linear and Nonlinear Viscoelastic Behavior Using Model Silica-Particle-Filled Polybutadiene. *Macromolecules* **38**, 8816 (2005).

[70] If N_p and V_p are respectively the total number and the volume of particles, and V is the volume of the system, the volume fraction of aggregates is $\phi = V_\mathrm{p}/V = 4\pi N_\mathrm{p}\sigma^3/3V$.

[71] The stress relaxation modulus is, up to a constant, the correlation function of the stress.

[72] Hyun, K., Kim, S. H., Ahn, K. H., Lee, S. J., Large amplitude oscillatory shear as a way to classify the complex fluids. *J. Non-Newtonian Fluid Mech.* **107**, 51 (2002).

[73] Cho, K. S., Hyun, K., Ahn, K. H., Lee, S. J., A geometrical interpretation of large amplitude oscillatory shear response. *J. Rheol.* **49**, 747 (2005).

[74] Ewoldt, R. H., Hosoi, A. E., McKinley, G. H., New measures for characterizing nonlinear viscoelasticity in large amplitude oscillatory shear. *J. Rheol.* **52**, 1427 (2008).

[75] Hyun, K., Wilhelm, M., Klein, C. O., Cho, K. S., Nam, J. G., Ahn, K. H., Lee, S. J., Ewoldt, R. H., McKinley, G. H., A review of nonlinear oscillatory shear tests: Analysis and application of large amplitude oscillatory shear (LAOS). *Prog. Polym. Sci.* **36**, 1697 (2011).

[76] Mermet-Guyennet, M. R. B., Gianfelice de Castro, J., Habibi, M., Martzel, N., Denn, M. M., Bonn, D., LAOS: The strain softening/strain hardening paradox. *J. Rheol.* **59**, 21 (2015).

[77] Hadizadeh, S., Linhananta, A., Plotkin, S. S., Improved measures for the shape of a disordered polymer to test a mean-field theory of collapse. *Macromolecules* **44**, 6182 (2011).

[78] The noise in the data prevents a more specific conclusion.

[79] Heinrich, G., Vilgis, T. A., A statistical mechanical approach to the Payne effect in filled rubbers. *EXPRESS Polym. Lett.* **9**, 291 (2015).

[80] Börzsönyi, T., Szabó, B., Wegner, S., Harth, K., Török, J., Somfai, E., Bien, T., Stannarius, R., Shear-induced alignment and dynamics of elongated granular particles. *Phys. Rev. E* **86**, 051304 (2012).

[81] Alizadehgiashi, M., Khabibullin, A., Li, Y., Prince, E., Abolhasani, M., Kumacheva, E., Shear-Induced Alignment of Anisotropic Nanoparticles in a Single-Droplet Oscillatory Microfluidic Platform. *Langmuir* **34**, 322 (2018).

[82] Yousefian, Z., Trulsson, M., Orientational arrest in dense suspensions of elliptical particles under oscillatory shear flows. *Europhys. Lett.* **136**, 36002 (2021).

[83] Corté, L., Chaikin, P. M., Gollub, J. P., Pine, D. J., Random organization in periodically driven systems. *Nature Phys.* **4**, 420 (2008).

[84] Payne, A. R., Whittaker, R. E., Dynamic properties of materials - Part II. Dynamic properties of clay-natural rubber vulcanizates. *Rheol. Acta* **9**, 97 (1970).

Supplementary Information for

"Microscopic Interpretation of the Payne Effect in Model Fractal-Aggregate Polymer Nanocomposite"

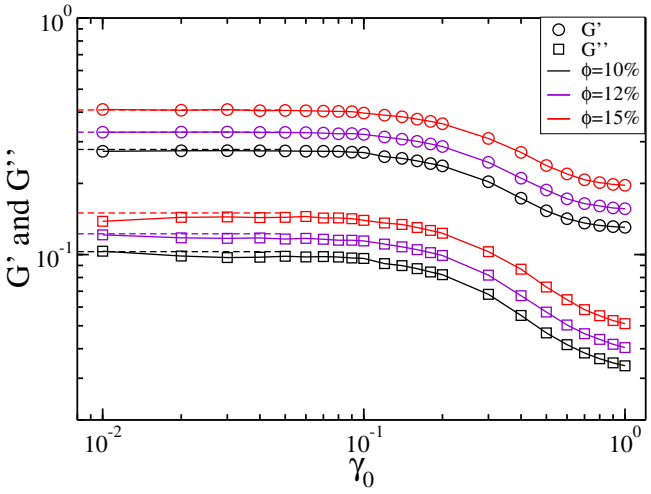

FIG. SM1. Influence of aggregate volume fraction: storage and loss moduli for various volume fraction ϕ. and aggregate size $\mathcal{N} = 20$. The dashed lines show the moduli computed from the Green-Kubo relation and equilibrium simulations [47].